Received: 29 July 2023 | Revised: 17 September 2023 | Accepted: 18 September 2023

DOI: 10.1002/pen.26515

RESEARCH ARTICLE

POLYMER ENGINEERING AND SCIENCE WILEY

Optimal design and operation of reactive extrusion processes: Modeling, model validation, and optimization algorithm

Maximilian Cegla | **Sebastian Engell**

Biochemical and Chemical Engineering Department, TU Dortmund University, Dortmund, Germany

Correspondence
Maximilian Cegla, Biochemical and Chemical Engineering Department, TU Dortmund University, Emil-Figge-Str. 70, 44227 Dortmund, Germany.
Email: maximilian.cegla@tu-dortmund.de

Funding information
EU Horizon 2020 programme SIMPLIFY, Grant/Award Number: 820716

Abstract

In this work, a methodology for the optimal design and operation of reactive extrusion processes in twin-screw extruders is presented. As a process model, a very accurate mechanistic finite volume twin-screw extruder model is used which is adapted to the reactive extrusion case. In the model, in contrast to other models, the pressure is described as a differential state in order to have a consistent set of equations. The model is compared to other models and advantages and disadvantages with respect to accuracy and computation time are discussed. For optimization, a memetic optimization algorithm (MA) that consists of a combination of a local optimization for the continuous operating parameters and an evolutionary algorithm (EA) for the global optimization of the discrete decision variables is employed to overcome the drawback of the longer model simulation time compared to simpler models. A reduction of optimization time by 90% for the MA compared to the EA was observed. The presented modeling and optimization methodology is validated on the widely investigated reactive extrusion process for ε-Caprolactone. The methodology is very flexible and the underlying model has good prediction characteristics, thus it is applicable to a wide range of reactive extrusion processes of industrial interest.

Highlights

- Simulation and optimization of reactive extrusion.
- Improved mechanistic twin-screw extruder model.
- Novel approaches for pressure and residence time modeling.
- Efficient combination of local and global optimization in a memetic algorithm.
- Benchmarking of the optimization results and performance with literature data.

KEYWORDS

extrusion, memetic algorithm, modeling, reactive extrusion, simulations

1 | INTRODUCTION

Reactive extrusion in twin-screw extruders combines the advantages of a multifunctional, continuous reactor with the excellent mixing performance and the flexibility of extruders. Although many products have been reported to be suitable to be produced[1] by reactive extrusion, only a handful have been commercialized. As reported by one of the leading suppliers of twin-screw extruders in 2016, only 87 extruders for reactive extrusion were sold in the past 50 years of which 64 were designed for the production of thermoplastic polyurethanes with an approximated production of 250.000 t per year.[2] This low number of industrial applications can be explained by the limitation of residence times, bad temperature control that might cause undesired side reactions, and the required knowledge of both the chemical reaction and the extrusion process.[3] Reactive extrusion offers a very energy-efficient production concept at different scales and enables the production of highly functionalized products, for example, polymers with carbon fibers or other fillers.[2] However, the traditional design of twin-screw extruders and the choice of the best operating parameters for the production of different products is time-consuming and costly, because it is mainly based on experimental trials. In reactive extrusion, besides the processing parameters such as barrel temperatures, throughput, or rotation speed, the choice of the screw design significantly influences the performance of the process. While it is possible to determine the optimal processing parameters approximately by experiments, testing many screw designs is infeasible as the number of possible combinations is very large. Therefore, to speed up process development and to obtain better solutions, a model-based process design and optimization approach is preferable. Another advantage of model-based optimization is the possibility of adapting the extruder to different products by characterization only of the chemical systems and then applying model-based optimization. For model-based optimization, suitable models are required. For the rheology of the materials, usually standard models are parametrized by experiments, for example, the Yasuda-Carreau model.[4] The chemical systems are usually described by ordinary differential equations which may be of high complexity to include all effects such as mass-transport efficiencies, the influence of temperature, and catalytic cycles. For polymerizations, often the method of moments is applied.[5] The extrusion model should therefore be able to embed complex models of the reaction chemistry. The extruder model must provide an accurate description of the residence time distribution (RTD) as a result of the internal flows over the length of the extruder. The RTD depends on the local progress of the reaction and the local temperature.[6] Vergnes et al.[7] proposed an extruder model based on a discretization of the extrusion volume into C-shaped elements with a description of the internal flows depending on the screw geometry. Gimenez et al.[8] extended the model of Vergnes et al.[7] to reactive extrusion and applied it to the reactive extrusion of ε-Caprolactone. A drawback of this approach is that the mass balances for the mass transport in the extruder and the reaction system are solved iteratively and separately to compute the final result. First, the extruder flows are computed from the direction of the die to the feed, under the assumption of a given distribution of the conversion, until the flow distribution converges to the melt temperature. Then the reaction system is simulated forward based on the calculated residence times and temperature from the first iterative solution. These two steps are iterated until convergence.[9] As a unique mapping between temperature, conversion, and local residence time is required, the reaction system and screw configuration can only be of a certain complexity. The local residence time has to be corrected iteratively,[10,11] and therefore a successful simulation cannot be guaranteed for complex systems. In contrast, our approach is based on the work of Eitzlmayr et al.[12,13] who proposed a mechanistic twin-screw extrusion model with finite volumes based on the characterization of screw elements by Kohlgrüber[14] for nonreactive pharmaceutical compounding applications. The approach has similarities to the model of Choulak,[15] which considers the extruder as a series of CSTRs. The model proposed by Eitzlmayr includes a very detailed and accurate description of the viscous dissipation for an accurate heat balance and computation of the local temperatures. In this work, the model by Eitzlmayr is extended for the reactive extrusion case so that complex reaction kinetics can be included. The RTD is provided by the internal flows between the finite volumes. From a chemical engineering perspective, a model based on the dynamic simulation of the extruder until a steady state is reached is favorable over a steady-state process model because multiple steady states can exist in reactive extrusion as reported by Janssen et al.[16] A drawback of our approach is longer computation times, which is compensated by an efficient optimization method. For the optimization of twin-screw extrusion processes, in the majority of the published works evolutionary algorithms (EA) are used.[17] Based on an EA and the modeling approach of Vergnes et al., optimizations of the screw configuration and of the operating parameters were carried out by Gaspar-Cunha et al.[18] and Teixeira et al.[19] using the simulation tool Ludovic©. In this work, we apply an evolutionary algorithm for the discrete decisions and extend it by a local optimization method for the continuous variables, leading to a memetic algorithm (MA).[20,21] The local optimization decreases the optimization times significantly by reducing the search space of the

EA and by reducing the number of infeasible solutions in the population of solutions. In a companion paper[22] the method proposed in this contribution is applied to the reactive extrusion of hydrophobically modified urethane paint additives, including the scale-up from an 18 mm laboratory extruder to a 75 mm production scale extruder.

2 | MODELING OF REACTIVE EXTRUSION PROCESSES

2.1 | Mass flow model

The modeling approaches to describe the internal flows within twin-screw extruders are based on the screw geometry[7] or empirical methods.[14] The geometry-based approach considers the screw channels as flattened out with a sliding barrel.[23] These two modeling approaches can be transformed into each other as they describe the same influences of the operating parameters of the process on the internal flows as shown in the Appendix A.

In this work, an empirical approach based on the work of Eitzlmayr et al.[12] is used. Figure 1 shows the discretization of the extruder into i finite volumes of length Δx with conveying and pressure-driven flows between each element. Δx can be chosen as the length of the shortest physical element or a multiple of it. The dynamics of the filling ratio f_i within a section of volume V_i with material of density ρ_i results from the mass balance of all incoming and outgoing flows of the section:

$$\frac{\partial f_i}{\partial t} = \frac{1}{\rho_i V_i}(\dot{m}_{\text{in},i} - \dot{m}_{\text{out},i}) \tag{1}$$

and the filling ratio is constant for a fully filled element in which a pressure builds up:

$$\frac{\partial f_i}{\partial t} = 0. \tag{2}$$

The switching of the dynamics of the elements between Equation (1) and the build-up of pressure is realized by branching during the simulation.

In a regular conveying volume V_i within an extruder of diameter D, for a rotation speed n, filling ratio f_i, density ρ, the conveying flow in forward direction $\dot{m}_{c,f,i}$ and backward direction $\dot{m}_{c,b,i}$ is described by Eitzlmayr et al.[12]:

$$\dot{m}_{c,f,i} = \rho \cdot f_i \cdot A_{1,f,i} \cdot n \cdot D^3, \tag{3}$$

$$\dot{m}_{c,b,i} = \rho \cdot f_i \cdot A_{1,b,i} \cdot n \cdot D^3. \tag{4}$$

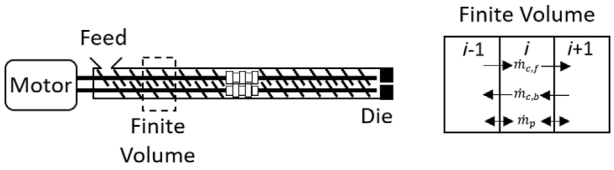

FIGURE 1 Schematic of the extruder discretized into finite volumes.

Typically only one screw parameter for conveying elements $A_{1,f,i}$ and $A_{1,b,i}$ is nonzero, indicating the conveying direction of the screw element. The nonzero screw parameter can be approximated using the cross-sectional area of the screw A_{cr} and the screw pitch T_s as proposed by Kohlgrüber et al.[24]:

$$A_{1,i} \approx \frac{A_{\text{cr}} \cdot T_s}{2 \cdot D^3}. \tag{5}$$

The second flow type is the pressure induced flow $\dot{m}_{p,i}$ which occurs if in an entirely filled element a pressure p_i has built up. The pressure-driven flow is especially important to overcome non-conveying screw elements such a shells, 90° kneading blocks, backward conveying elements or the die. The resulting pressure flow is a function of the pressure drop Δp_i, the dynamic viscosity η_i, the diameter D and the proportionality factor $\frac{A_{1,i}}{A_{2,i}}$ that describes the pressure drop depending on the geometry of the screw element. The resulting pressure flow that moves the material in the direction opposite to the pressure gradient is described by:

$$\dot{m}_{p,i} = \rho \cdot \frac{A_{1,i}}{A_{2,i}} \cdot \frac{D^4}{\eta_i} \cdot \frac{\Delta p_i}{\Delta x}. \tag{6}$$

As suggested by Eitzlmayr et al.[12] A_2 can be approximated well by a linear interpolation of measured data:

$$A_{2,i} \approx -93.4 \cdot \frac{T_s}{D} + 893. \tag{7}$$

The conveying and pressure drop characteristics of mixing elements such as screw mixing elements (SME), turbine mixing elements (TME), or tooth mixing elements (ZME) are assumed to be proportional to the characteristics to the regular elements with the same pitch and diameter. The SME is a conveying element with gaps milled into the flights to allow a back-flow, whereas the ZME is a left-handed element with teeth at the flight to generate a forward conveying capacity even though being left handed. A TME section considered here consists of right-handed gears alternating with empty shells. For a 30 mm extruder such mixing elements were investigated

by Brouwer et al.[25] The parametrization of different kneading blocks was investigated by Bauer using smoothed particle hydrodynamics simulations[26] and Stritzinger using a numerical modeling approach.[27,28] To calculate the mass balances for several species, the mass flows are multiplied by the weight fractions w_i in each element. This formulation can be extended to the reactive case by including the reaction rate r_i to take into account the weight fraction changes due to the chemical reaction:

$$\frac{\partial w_i}{\partial t} = \frac{1}{f_i \cdot V_i \cdot \rho_i}\left(w_{i-1} \cdot \sum_{i-1\rightarrow i} \dot{m} \cdot w_{i-1} + \sum_{i+1\rightarrow i} \dot{m} \cdot w_{i+1} - \sum_{i\rightarrow i-1} \dot{m} \cdot w_i - \sum_{i\rightarrow i+1} \dot{m} \cdot w_i \right) + \frac{w_i}{f_i} \cdot \frac{\partial f_i}{\partial t} - r_i. \quad (8)$$

For the elements with external feeds into the extruder, these contributions also have to be considered in the mass balance. For the first simulation, an initial distribution of the weight fractions is assumed. The reaction rate has to be determined as a function of concentrations and temperature for each species of the reaction system. Besides the concentrations, quantities such as conversion or molecular weight can be treated as concentrations of pseudo components. This enables to include the description of such quantities at any location and point in time and to compute the RTD, by feeding a pseudo-component as an impulse at the inlet and monitoring the response at the die.

2.2 | Residence time model

Using the description of the internal flow as shown in the previous section, it is not possible to represent the RTD when using mixing elements or in the case of large clearance between extruder screw and barrel. This model only takes into account the overall conveying of material in the main conveying direction and neglects the fraction of the transported material that moves into the opposite direction. The model thus is only valid for a screw configuration with only simple forward conveying elements, as presented in Reference [29] for the reactive extrusion case, for which the axial dispersion model shows good accordance with experimental results. The presence of mixing elements causes a tailing of the RTD that cannot be described by the RTD that is generated by a cascade of continuous stirred tank reactors (CSTR).[25] This is the case as due to the choice of the discretization, the number of elements can vary, for example, between 20 and 200 which is affecting the RTD. Using the relation between the number of CSTRs and Bodenstein number Bo proposed by Elgeti[30] this value corresponds to Bo = 11 (large dispersion) and Bo = 101 (small deviation from plug flow).[31] Especially in reactive extrusion systems, the product quality not only depends on the mean residence time but also on the RTD. Therefore, in Reference [32] it was proposed to extend the model by including both the forward and the backward conveying capacity of the extruder model by using the analogy to the back-flow cell model (BCM). This model was first introduced as a mathematical model to describe the RTD of reactor networks with back-flows by Roemer and Durbin.[33] The BCM was used for the description of the RTD for twin-screw extruders by Choulak et al.[15] but only for a description of the overall RTD based on experimental data, not for predicting the internal flows and the local RTD. The inclusion of bi-directional flows enables a description and prediction of the macroscopic mixing based on RTD data for the individual screw elements. A drawback is that the characterization is accurate for a given discretization of the system into finite volumes, as this represents the number of continuously stirred tank reactors in series in the BCM. By applying this approach to our model, the conveying flow parameters of a screw element are described by $A_{1,f,i}$ or $A_{1,b,i}$ for the flow in the main conveying direction and a back-flow ratio σ_B. Thus the applied forward and backward conveying parameters $A'_{1,f,i}$ and $A'_{1,b,i}$ in the model are described by:

$$A'_{1,b,i} = \sigma_B \cdot A_{1,f,i}, \quad (9)$$

$$A'_{1,f,i} = A_{1,f,i} + A'_{1,b,i}. \quad (10)$$

The overall mass balance of a finite volume is not affected by this modification, but the residence time of an element in the extruder changes. For the calculation of the proportionality factor for the pressure flow $\frac{A_1}{A_2}$, the unmodified A_1 is used. The results of this extension of the model were presented for several types of screw elements and kneading blocks in Reference [32].

A representative result of the application of this modeling approach is shown in Figure 2. The number of elements is fixed to 10 elements for both the CSTR-based approach as well as the BCM. With the optimal back-flow ratio of 0.68, the model describes the RTD very accurately. Considering the geometry of the element with gaps milled into the flanks of the screw elements, this value appears reasonable. Especially the tailing of the distribution as well as the width of the distribution are represented excellently by the proposed method, which provides an alternative to computationally expensive computational fluid dynamics simulations, for example, by smoothed particle hydrodynamic calculations of mixing rates of the elements as proposed by Eitzlmayr et al.[34] The results for more mixing

elements and kneading blocks with different staggering angles are shown in Table 1. The back-flow ratios were determined by solving an optimization problem, minimizing the deviation between the model prediction and the experimental points for the RTDs of the different elements. For all elements with back-mixing, the proposed method significantly outperforms the RTD description by a CSTR cascade. Therefore, the proposed method gives the model an additional degree of freedom to describe the internal flows more accurately, based on the results from experimental RTD investigations.

2.3 | Novel pressure model

A critical aspect for the prediction of the operation of extrusion equipment is a precise prediction of the back-pressure zones within the equipment, as this influences the RTD, the temperature and the viscosity of the product. The calculation of the pressure within a twin-screw extruder can be performed by several different approaches. One approach is to fix the length of the pressurized zone based on measurements and experience as proposed by Ganzeveld et al.[36] for the reactive extrusion case of the polymerization of butylmethacrylate. Another approach is to compute the lengths of fully filled zones and consider dynamic boundaries for these as proposed by Kim and White.[37] The downside of this approach is that its not easily applicable to the reactive extrusion case, as the length of starved zone is determined by integration and the melt properties, and consequently the pressure drop change not only due to temperature changes but also due to chemical conversion. Another option is the consecutive iterative calculation of the internal flows within the entire extruder starting at each restrictive element until the pressures match the flow pattern as implemented in the software Ludovic©.[7] This requires a definition of restrictive elements, but this definition may vary depending on throughput, speed of rotation, local melt temperature, and viscosity. Alternatively, the pressure can be calculated as the solution of the linear system of equations to fulfill the mass balances within the pressurized section, as proposed by Choulak et al.[38]:

$$\overline{A} \cdot \overline{p} = \overline{b}. \tag{11}$$

In this formulation, $\overline{p}$ represents the pressure vector of all fully filled elements, $\overline{A}$ is a sparse banded matrix describing the resulting pressure flows as functions of local melt properties and screw geometry and $\overline{b}$ is the vector of the conveying flows in each section. For each step within the integration, the system of linear equations has to be solved because with varying viscosity the pressure characteristics change and have to be re-computed. To overcome this limitation, we suggest the use of the singular perturbation approach to describe the pressure

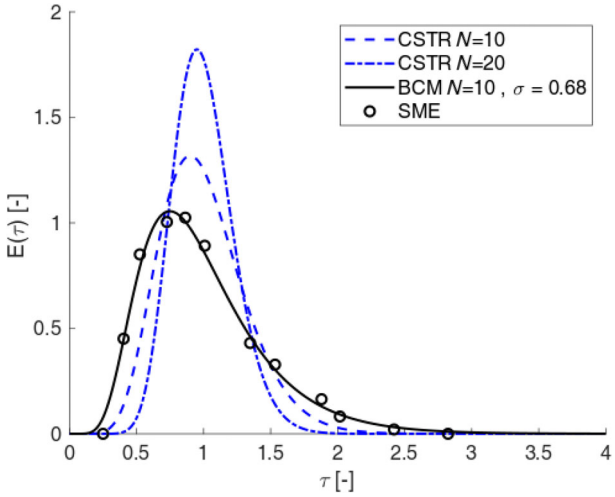

FIGURE 2 Comparison of the traditional CSTR cascade model with the proposed extended back-flow cell model for an extruder section of 100 mm length consisting of screw mixing elements (SME). The experimental RTD data for the SME elements was taken from Reference [25].

TABLE 1 Results of the application of the BCM method[35] for different screw elements and $N = 10$ finite volume elements.

Screw element	σ_B [−]	Error BCM [−]	Error CSTR cascade [−]
SME[a]	0.684	0.074	4.521
TME[a]	0	3.848	3.848
ZME[a]	0.040	0.364	0.391
+60°KB[b]	0.247	2.856	4.837
+30°KB[b]	0	2.521	2.521
−30°KB[b]	0.497	1.580	6.263
−60°KB[b]	0.456	1.475	6.078

Note: The experimental data was taken from [a]Brouwer 2002[25] and [b]Poulesquen 2003.[10] The total error is the summation of the squared differences between BCM and the augmented experimental data for RTD's. The experimental data is augmented by linear interpolation to obtain 100 equidistant data points.

as a state with a very fast dynamics which converges to the value for which the mass balance is fulfilled:

$$\frac{\partial p_i}{\partial t} = c\frac{1}{\rho_i V_i}\left(\dot{m}_{f,i-1} + \dot{m}_{b,i+1} + \dot{m}_{p,i-1} - \dot{m}_{p,i} - \dot{m}_{f,i} - \dot{m}_{b,i}\right). \tag{12}$$

The constant c in Equation (12) has to be quantified. Practically speaking it is the rate of change of the pressure for a given deviation of the mass flows from the steady state.

For large values of c, the dynamic and the steady state error converge below the measurement accuracy for typically used equipment. Note that the die volume is in practice one or two magnitudes smaller than the volume of a regular screw element. The resulting effect on the dynamics can be compensated by assuming similar dynamics for the die as for the last screw-element.

In Figure 3 the effect of the variation of the dynamic constant is shown for the dynamic behavior of the die pressure and the mass balance error at the start-up of an extruder. Initially, the extruder is assumed to be filled with a filling ratio of 60% to test the proposed method. The initial overshooting at 20 s can be explained by the coupling of the dynamics of temperature and pressure. With increasing temperature, the viscosity of the melt decreases and consequently, the pressure drop at the die decreases. After the initial start-up phase, more melt is pushed through the die increasing the pressure again. For all three dynamic constants, no steady-state offset of the pressure was observed after 300 s. The integrated mass balance error was determined by monitoring the weight fraction balance in the last screw element before the die. The results showed an overshoot of the concentration in the element for all cases which indicates a slight underestimation of the pressure. While for the cases of $c = 10^8$ Pa and $c = 10^9$ Pa, the pressure dynamics at the die were not distinguishable, the integrated mass balance error still showed a significant improvement. We typically apply $c = 10^9$ Pa for the dynamic constant. Increasing the dynamic constant further leads to higher simulation times, as the dynamics become more ill-conditioned. The proposed pressure calculation is only performed for the cases of a fully filled element or of an already existing pressure, as the filling of an element must not generate a pressure increase. Otherwise, Equation (13) is applied:

$$\frac{\partial p_i}{\partial t} = 0. \tag{13}$$

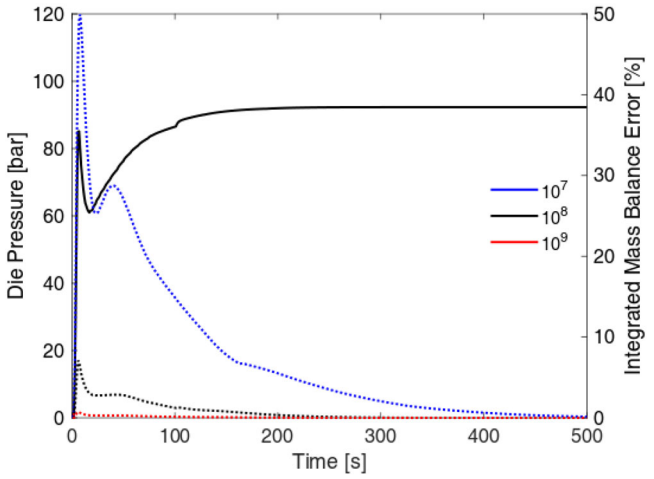

FIGURE 3 Effect of the variation of the dynamic constant on the evolution of the absolute pressure (solid) as well as on the mass balance error integrated over the length of the pressurized zone (dotted) for the start-up of the extrusion.

2.4 | Thermal model

The melt temperature T_m in each element is calculated by solving the local energy balance.

The temperatures have an influence on the dissipated mechanical energy $\dot{Q}_{\text{diss}}$ within the element. The melt is assumed to have a specific heat capacity c_p. Heat transfer takes place between the barrel and the melt, described by $\dot{Q}_{bm}$. The reaction introduces the energy flow $\dot{Q}_{\text{reaction}}$ into the system, each reacted mole releases the heat of reaction—ΔH. Thus, the temperature balance for the melt is:

$$\frac{\partial T_{m,i}}{\partial t} = \frac{1}{\rho_i V_i c_p f}\left(\dot{Q}_{bm} + \dot{Q}_{\text{diss}} + \dot{Q}_{\text{reaction}} + \sum T_{m,i}\cdot\dot{m}_i\cdot c_{p,i}\right) - \frac{\partial f}{\partial t}\cdot\frac{T_{m,i}}{f_i}. \tag{14}$$

The barrel temperatures are assumed to be constant over a section, as this is the case in practice. The temperatures are regulated by electrical heating rods and cooling water. The heat transfer coefficient between the barrel and the melt is calculated by the empirical correlation developed by Todd[39]:

$$h_{Tb} = 0.69\cdot\frac{\lambda}{D/2}\cdot\left(\frac{(D/2)^2\cdot n\cdot\rho}{\eta}\right)^{0.28}\cdot\left(\frac{c_p\cdot\eta}{k}\right)^{0.33}\cdot\left(\frac{\eta}{\eta_w}\right)^{0.14}. \tag{15}$$

The resulting heat transfer between barrel and melt $\dot{Q}_{bm}$ is calculated by:

$$\dot{Q}_{bm} = h_{Tb} \cdot A_{bm} \cdot \left(T_i^B - T_i^M\right) \tag{16}$$

with the barrel surface A_{bm} and the barrel and melt temperatures T_i^B and T_i^M.

The introduced mechanical energy $\dot{Q}_{\text{diss}}$ is calculated as proposed by Eitzlmayr et al.[13] with contributions of the axial viscous dissipation $\dot{q}_{\text{diss,ax}}$ and a radial dissipation $\dot{q}_{\text{diss,r}}$:

$$\dot{Q}_{\text{diss}} = V_i \cdot f_i \cdot \left(\dot{q}_{\text{diss,ax}} + \dot{q}_{\text{diss,r}}\right). \tag{17}$$

The axial dissipation is caused by the energy loss of the pressure-driven flow[13]:

$$\dot{q}_{\text{diss,ax},i} = \frac{D^4}{K_{p,i} \cdot \eta_i \cdot A_{\text{cr}}} \cdot \left(\frac{\Delta p_i}{\Delta x}\right)^2, \tag{18}$$

where A_{cr} denotes the free cross-sectional area of the twin-screw in the barrel. The radial viscous dissipation consists of dissipation within the gap between screw and barrel and in the bulk region. The dissipation in the gap can be calculated by Eitzlmayr et al.[13]:

$$\dot{q}_{\text{diss,gap},i} = \eta_i \cdot \gamma_{\text{gap}}^2 = \eta_i \cdot \left(\frac{D \cdot \pi \cdot n}{h}\right)^2 \tag{19}$$

with the clearance between screw and barrel h. The dissipation in the bulk region is calculated by Eitzlmayr et al.[13]:

$$\dot{q}_{\text{diss,bulk},i} = 4\eta_i \cdot \gamma_{\text{bulk}}^2 = 4\eta_i \cdot \left(\frac{D_c \cdot \pi \cdot n}{H_{av}}\right)^2 \tag{20}$$

with the core diameter of the screw elements D_c and the cross-sectional area of one screw H_{av}. To obtain the total radial dissipation $\dot{q}_{\text{diss,r}}$, both contributions are weighted by the volume fractions ϵ_{gap} and ϵ_{bulk} as well as by the actual filling ratio f_i[13]:

$$\epsilon_{\text{gap}} = 1 - \epsilon_{\text{bulk}} = \frac{\alpha \cdot D \cdot h \cdot n_F}{A_{\text{cr}}}, \tag{21}$$

$$\dot{q}_{\text{diss,r}} = \dot{q}_{\text{diss,gap},i} \cdot \epsilon_{\text{gap}} + \frac{\dot{q}_{\text{diss,bulk},i} \cdot \epsilon_{\text{bulk}} \cdot f_i}{\epsilon_{\text{gap}} + \epsilon_{\text{bulk}} \cdot f_i} \tag{22}$$

with the tip angle α and the number of flights n_F. This detailed calculation of the viscous dissipation provides a very accurate prediction of the temperature profile.

2.5 | Summary of the model

The presented model is a combination of existing and new models that describe the different effects that are present in a reactive twin-screw extruder. The core of the model is the flow model. For reactive extrusion, the C-shaped discretization has been extensively studied and validated with experimental results. Our mechanistic modeling approach and the C-shaped modeling approach can be transferred into each other as shown in the appendix. The effects of a conveying and pressure-driven flow have similar dependencies on the melt viscosity and the rotation speed. The complex geometrical correction factors proposed by Vergnes et al.[7] can be lumped into the factors A_1 and A_2. The comparison of the quantitative results from different publications using one or the other model also shows comparable results as also shown in the Appendix A.

The adjustment of the pressure model using the singular perturbation approach with finite pressure dynamics instead of the calculation of the pressure as a system of equations does not influence the simulation results significantly, especially if the simulation time is sufficiently long and the dynamic constant is chosen sufficiently fast. In practice, the dynamic measurement of the pressure is limited by the accuracy of the pressure sensor, the inertia of the pressure sensor to temperature effects, and the sampling rate of the data acquisition system.

The description of the RTD is improved by the application of the BCM. Whereas in regular extrusion processes, the RTD is not critical, it is essential in reactive extrusion. With the modeling approach presented here, it is possible to accurately adjust the internal flows to match the overall RTD. The overall flows and therefore the resulting local filling levels in the elements are not affected. For the extreme case of no back-flow, the established model corresponds to the original mechanistic model. The RTDs reported in the literature with tailing are described in a coherent model considering local effects such as viscosity and operating conditions.

The modeling of the progress of the reaction via the component balance follows the approach for any flow-based chemical reactor[31] and the contribution of the heat of reaction as a function of the reaction rate to the local heat balance is included. The challenge in terms of reaction modeling is the measurement and determination of the reaction kinetics.

Regarding the reaction kinetics, the quality of mixing can contribute significantly to the observed progress of the reactions compared to a purely kinetic model. In contrast to the large batch reactors with poor mixing, the kinetic models valid for industrial-scale reactive

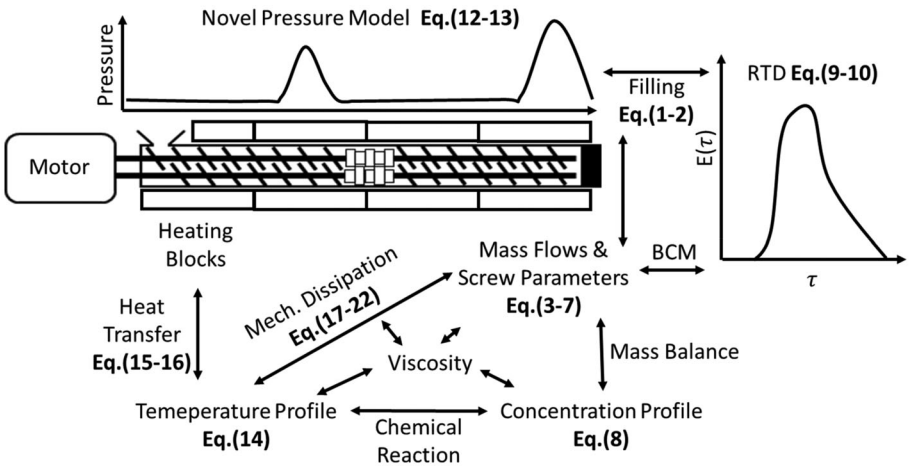

FIGURE 4 Overview of the proposed reactive extrusion model with the main phenomena and their connections. For simplicity, the influences of the operating conditions are omitted. An example for the chemical reaction and rheological system is given in Section 4.1.

extrusion can be determined by laboratory scale experiments, due to the high mixing intensity within the twin-screw extruder. To summarize, the proposed model offers an enhanced representation of the entire process by combining well-known partial models and components. This combination allows for individual validation and description of the effects, resulting in an improved understanding of the overall process and is graphically summarized in Figure 4.

3 | OPTIMIZATION

3.1 | Memetic optimization

For the optimization of the configuration and the operating parameters of a reactive extrusion process, it is proposed in this work to use a MA used in contrast to an evolutionary algorithm as in References [18,40,41]. MAs combine a global search by a metaheuristic (here an evolutionary algorithm) with a classical local optimization algorithm. This overcomes the weakness of EAs to be inefficient around local optimal as well as the restriction of classical optimization algorithms to only provide local optima. The EA can perform a global exploration of new regions of the search space and the gradient-based local optimization then converges quickly to the best points in these regions. Such algorithms have been used successfully in the design optimization of chemical processes.[20,21] Crepinsek et al.[42] also point out that this approach offers a good trade-off between exploration of the search space and exploitation by local optimization. Gaspar-Cunha et al.[18] reported good results with the use of the Inver-over operator that was proposed by Tao in 1998[43,44] for the solution of the traveling salesman problem, which is structurally similar to the optimization of the screw configuration. The conclusion of Reference [18] was that the description of further screw geometries and a higher model complexity were desirable. By using the MA in combination with the model that was described in Section 2, it is possible to optimize reactive extrusion processes with variable screw geometries based on a high-accuracy model.

The structure of the optimization algorithm is depicted in Figure 5. The optimizer is initialized with a random population of size N_{Pop} in generation $i = 0$. Each individual in the population contains the encoding of a complete screw configuration and continuous optimization variables such as the throughput, the speed of rotation, or barrel temperatures. The integer variables in the encoding represent the locations of screw elements (type and length) on the extruder shaft from a predefined set. Within an individual, every location can only be assigned once. Afterward the population is evaluated and the optimization of the continuous optimization variables such as throughput, barrel temperature, or speed of rotation is performed. The resulting performance is assigned as the fitness value to each individual (i.e., screw design and operating parameters) in the population and if continuous variables are optimized locally, the optimal continuous variables are assigned to the individual. In case of a failed simulation or an infeasible solution, the value 10^{10} is assigned to the fitness of the individual. In the last step, satisfaction of the termination criterion is checked. We typically applied the number of generations N_{Gen}, but commonly also stagnating best fitness values or numbers of generations without improvements are used.[45] In case the algorithm is not terminated, the parents and survivors are selected. As potential parents, all individuals in the population are selected. From the population, first, the elites with the best fitness values are selected for survival. The size of the elites is defined as a percentage of the total population. The other individuals of the next generation are generated by using the Inver-

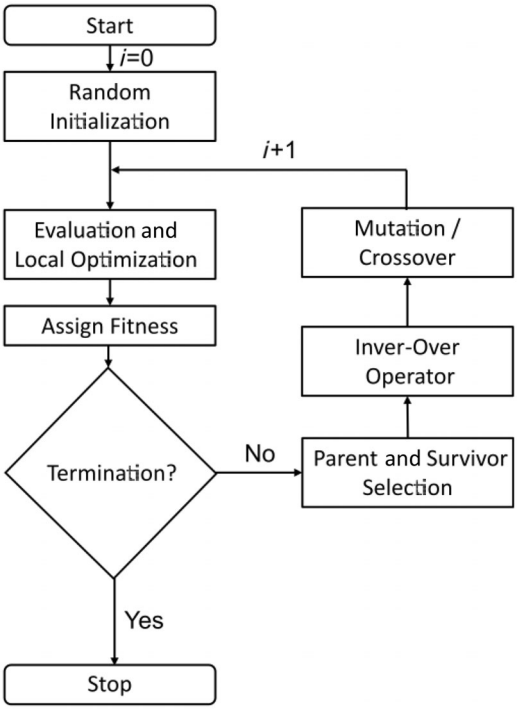

FIGURE 5 Flowchart of the memetic optimization algorithm.

over operator. The operator is a combination of the inversion operator and the crossover operator. With a certain Inver-over probability, a random section in the genome is inverted, otherwise, the regular crossover is applied and the position of two adjacent elements is changed. An example of application of the Inver-over operator is shown in the appendix in Figure A2.

In the case of the optimization of continuous variables which are not optimized by the local optimization, mutation and crossover are performed on the entire population. For mutation, the old variable is replaced with a mutation probability by a new random value within the bounds of the variable. For crossover, with a certain crossover probability, the value is replaced by the value of the same variable of a random individual in the population. The generation number i is increased by one and evaluated. The parametrization of the algorithm that is used for the example in Section 4 is shown in Table 2.

For the simulation and evaluation of each configuration, the system is described by the model discussed in Section 2 as an ODE system in the symbolic framework CasADi[46] and the local solver fmincon is used in MATLAB for the local optimization. The steady-state operating points that determine the performance of an individual are obtained by simulating the dynamic model for a sufficiently long time horizon. This dynamic simulation within the optimization ensures that the resulting operating points can be attained in operation and are not unstable equilibrium points. In a later stage during the operation of the process, the same dynamic model can be used to visualize and monitor the process, as well as in a model-based process control scheme. Using consistent models for process design, optimization, and control helps to reduce the development time to an optimized production for a new product significantly.

TABLE 2 Parametrization of the memetic optimization algorithm.

Parameter	Description	Value
N_{Pop}	Population size	100
N_{Gen}	Number of generations	50
P_{Elites}	Percentage of elites	20%
$P_{\text{Inver-over}}$	Inver-over probability	25%
P_{Mutation}	Mutation probability	20%
$P_{\text{Crossover}}$	Crossover probability	20%

3.2 | Cost function

The cost function used in the optimization can be chosen freely from maximizing the throughput to complex nonlinear economic cost functions. Moreover, constraints can be formulated and implemented both in the local and in the global optimization. The cost function and constraints can contain any variable of the simulation model. An example for a cost function is the energy introduced into the process by electrical power for heating and for the electrical drive of the extruder per total throughput:

$$min \frac{\dot{Q}}{\dot{m}_{\text{total}}} \tag{23}$$

$\dot{Q}$ is the sum of the mechanical energy that is provided to the melt by the viscous dissipation and the thermal energy that is introduced by heating the barrel:

$$\dot{Q} = \dot{Q}_{bm} + \dot{Q}_{\text{diss}} \tag{24}$$

with the contributions calculated as described in Section 2.4.

4 | APPLICATION TO THE ε-CAPROLACTONE POLYMERIZATION

For the validation of the modeling and optimization, the reactive extrusion of ε-Caprolactone is used. This process

was investigated by Gimenez et al.[8,47–49] and optimizations were performed for the operating conditions and screw design by Gaspar-Cunha et al.,[18] Berzin et al.,[50] and Teixeira et al[40] The previous work on this system and the availability of data enables allows for a comparison of both modeling and optimization results. Polycaprolactone is a biodegradable polyester that is mainly used in biomedical applications.

4.1 | Chemical model

The polymerization of ε-Caprolactone is a ring-opening polymerization initiated by an by the metal complex titanium isopropoxide. The reaction kinetics of the polymerization can be described as[51]:

$$\frac{d[M]}{dt} = -1.2 \times 10^{16} \cdot [M] \cdot [I_0]^{\alpha} \exp\left(\frac{-E_a}{RT}\right) \tag{25}$$

with the concentration of the monomer $[M]$, the initial initiator concentration $[I_0]$, the activation energy E_a of the reaction, the temperature T and the universal gas constant R. The weight average molecular weight M_w is a function of the conversion X and the monomer to initiator ratio $[M0]/[I0]$ and can be described by Poulesquen et al.[52]:

$$M_w = X \cdot (39 \cdot [M_0]/[I_0] + 7900) + 114. \tag{26}$$

The conversion of the monomer, X is a function of the monomer concentration M and the initial monomer concentration M_0 and is described by Poulesquen et al.[52]:

$$X = \frac{M_0 - M}{M_0}. \tag{27}$$

A value of 0 represents no conversion, and a value of 1 full conversion of the monomer. The zero shear viscosity η_0 of this system can be described by a generalized cross-Carreau equation as proposed by Gimenez et al.[8]:

$$\eta_0 = 1.35 \times 10^{-17} \cdot \exp\left(\frac{E_v}{R} \cdot \left(\frac{1}{T} - \frac{1}{T_0}\right)\right) \cdot M_w^{4.4} \tag{28}$$

with the activation energy E_v.The viscosity as a function of the shear rate $\dot{\gamma}$ is given as Poulesquen et al.[52]:

$$\eta(\dot{\gamma}) = \frac{\eta_0}{\left[1 + (\tau \cdot \dot{\gamma})^a\right]^{(1-p)/a}} \tag{29}$$

with the pseudoplastic index a and the power index p. The relaxation time τ is computed by Gimenez et al.[8]:

$$\tau = 1.7 \times 10^{-20} \exp\left(\frac{E_v}{R}\left(\frac{1}{T} - \frac{1}{T_0}\right)\right) \cdot M_w^{4.1}. \tag{30}$$

The parameters of the chemical system are presented in Table 3.

4.2 | Extruder

The co-rotating twin-screw extruder is the integral part of the reactive extrusion process. To validate the twin-screw extruder model and the performance of the optimization algorithm, the results are compared with published results for the ε-Caprolactone process in References [18,40,50]. The extruder is the same as in the references, a Leistritz 30.34 extruder with a L/D ratio of 36. The geometric parameters of the extruder are presented in Table 4.

4.3 | Optimization results

The degrees of freedom of the optimization is the rotation speed within a range of 150–200 rpm, the throughput between 3 and 30 kg/h, and the barrel temperature in the range of 140–180°C as well as the screw geometry. Three different cases are studied with different monomer-to-initiator ratios of 400, 800, and 1200. The details of the rheological and chemical system of the ε-Caprolactone polymerization were given in Section 4.1. The parameters of the EA are given in Table 2. For of the reactive extrusion of ε-Caprolactone, the energy demand of the process per mass of product is used as the cost function (Equation (23)) to be directly comparable to Reference [18]. The constraints are a conversion larger than 99.9%, a maximum bulk melt temperature of at most 220°C, a maximum melt temperature of 210°C at the die, and a total dissipated energy of at most 9200 W. The constraint on the conversion is not active as full conversion is achieved already after about 30% of the extruder length for the full range of operating conditions. The specific energy demand was also selected as optimization criterion as it represents an economic cost function for the process which is important during process development. The performance measures such as the maximum pressure or temperature, residence time, or restrictions to the individual specific energy contributions can be directly considered within our optimization method through the constraints and were chosen for this case as shown before.

The screw elements that can be placed by the optimizer are shown in Table 5. Only the locations of the elements that are underlined in Table 5 can be changed.

TABLE 3 Parameters of the polymerization model of ε-Caprolactone.[8,51]

Parameter	Description	Value	Unit
ΔH	Reaction enthalpy	−250	J/g
M_0	Molecular weight of the monomer	114	g/mol
ρ	Density	1210	kg/m^3
E_a	Activation energy of the reaction	92.6	kJ/mol
E_V	Activation energy of the rheology	40.0	kJ/mol
α	Chemical order of the initiator	3.25	-
R	Universal gas constant	8.314	J/mol
T_0	Reference temperature	120	°C
p	Power index	0.52	-
A	Pseudoplastic index	1.25	-

TABLE 4 Geometrical parameters of the Leistritz 30.34 extruder.

Parameter	Description	Leistritz 30.34
D	External screw diameter [mm]	33.8
D_C	Internal screw diameter [mm]	26.2
C_L	Centerline distance [mm]	30
$\frac{L}{D}$	Length/diameter ratio [−]	36
L	Screw length [m]	1.2

Similar to,[18] for the optimization of the screw geometry the first two screw elements are fixed to ensure a reliable introduction of the material feed into the extruder. The elements 11, 12 and the die are fixed to ensure a comparable pressure build-up as the pressure is used as indicator for the viscosity. The elements 3–10 can be distributed freely by the optimizer. The extruder is discretized into units of 30 mm length matching the minimum length of the available screw elements. Compared to,[53] the length of the die was increased to 30 mm and the diameter of the die was changed from 2 to 2.63 mm to obtain the same pressure drop. Instead of using six kneading blocks with various lengths a staggering angle of 90°C and a width of the disc of 7.5 mm, the optimization was carried out with four kneading blocks with a length of 30 mm per block and four discs each to be compatible with the discretization. The total length of the kneading blocks is unchanged compared to Reference [53]. The parametrization of the conveying and pressure characteristics is shown in Table 6. These values result from Equations (5) and (7).

Initial computations showed a limitation by the pressure drop caused by the diameter of the die. The pressure at the die reached a value of 120 bars at a throughput of 23 kg/h, generating a back-pressure zone over the entire length of the extruder. Therefore, higher throughputs were not feasible. These results are consistent with the outcome of the study in Reference [18] where the results of the Pareto optimization show a maximum feasible throughput of 23 kg/h at 200 rpm for all monomer to initiator ratios considered. The observation of this effect at the same throughput and similar temperatures indicates the consistency with the pressure drop calculations of the reference.

Consequently, for further investigation, a diameter of the die of 5 mm was chosen. The maximal achievable throughput resulted as 35 kg/h reaching the maximum process temperature of 220°C in accordance with the result in Reference [53] using Ludovic©. The only difference between the two simulation models is that the viscous dissipation is estimated slightly higher by Ludovic©. The optimization is limited by the same bounds in the operating space of rotation speed and throughput as presented in Reference [53]. The results of the optimization using the MA for the three different cases and the optimal operating conditions are shown in Table 7 and the corresponding optimal screw configurations are depicted in Figure 6.

For the cases of $[M0]/[I0]$ ratios of 400 and 800, the optimal operating conditions, with respect to the specific energy demand, are at the maximum throughput of 30 kg/h, 150 rpm, and a barrel temperature of 180°C. With an increase of the $[M0]/[I0]$ ratio to 1000, the energy introduction by viscous dissipation is significantly higher and requires lowering of the barrel temperature to 160.2°C to provide additional cooling of the melt to satisfy the constraint of a temperature of 210°C at the die. Due to the increasing product viscosity, the specific energy demand per kg of product rises from 0.248 MJ/kg for an $[M0]/[I0]$ ratio of 400 to 1.027 MJ/kg for a $[M0]/[I0]$ ratio of 1000. Comparing the different screw configurations for the different monomer to initiator ratios, the biggest difference is the positioning of the kneading

Parameter	1	2–3	4–5	6	7–10	11	12	Die
Length [mm]	300	120	120	120	30	120	60	30
Element	R20	R45	R30	R20	KB90	R20	R30	Ø5

Note: The positions of the underlined elements can be changed by the optimizer, the elements 1, 2 (extruder inlet zone), and 11–13 (extruder die section) are fixed. R30 and L30 indicate forward (to the die) and reverse (to the feed) conveying elements with a pitch of 30 mm. KB90 indicates kneading blocks with a staggering angle of 90°. A round die of 30-mm-length and 5-mm-diameter is used.

TABLE 5 Set of screw elements for the ε-Caprolactone case.

TABLE 6 Flow and pressure characteristics of the screw elements for the Leistritz 30.34 compounder.

Screw element type	Length [mm]	A_1	A_2	σ_{BCM}
20/20 R	30	0.1111	838	0
30/30 R	30	0.1667	810	0
45/45 R	30	0.2500	769	0
KB 90/4/30	30	0	1214.4	0

[M0]/[I0] [−]	$\dot{m}$ [−]	n [rpm]	T^B [°C]	Energy input [MJ/kg]	T_{max} [°C]
400	30	150	180.0	0.248	188.5
800	30	150	180.0	0.694	210.0
1000	30	150	160.2	1.027	210.0

TABLE 7 Optimal operating conditions for the monomer to initiator ratios of 400, 800, and 1000 and the screw configurations in Figure 6.

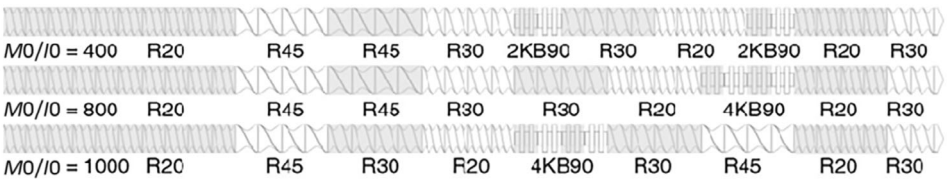

FIGURE 6 Optimal screw configurations (minimal specific energy requirement) for monomer-to-initiator ratios of 400, 800, and 1000. The numbers indicating the different sections are shown in Table 5.

blocks. As they are not actively conveying with a staggering angle of 90°, they build up a restrictive pressurized zone. For a [M0]/[I0] ratio of 400, the optimal configuration is to have two separate sections of kneading blocks at the start and at the end of the extruder. For a [M0]/[I0] ratio of 800, the optimal configuration is to have all kneading blocks located consecutively at the last possible location of the extruder. Reducing the initiator concentration further, the optimal position of the kneading blocks is closer to the feeding port. A similar effect for the screw placement was also observed in the reference work[40] for the maximization of the throughput under the given processing conditions.

Figures 7 and 8 show the pressure, filling level, viscosity, temperature, and conversion profiles over the length of the extruders and the RTD for the optimal solutions. For the case of a [M0]/[I0] ratio of 400, the section between the two kneading blocks is almost entirely filled despite having conveying elements between the blocks. Due to more viscous dissipation, a higher melt temperature is reached which is lowering the viscosity and the heat transfer from the barrel. A pressure of about 5 bar is reached at the die with an almost linear pressure decrease. For the case of lower initiator concentrations, the pressure is increased to 17 and 28 bar. This is caused by the higher viscosity of the polymer as with less initiator fewer chains with higher molecular weights are formed. The positions of the kneading blocks are visible in the pressure profile by pressure peaks. As the throughputs, the rotation speeds, and the length of the backpressure zones are similar for different cases, the resulting RTDs are almost identical. The mean residence times are 47 s for [M0]/[I0] = 1000 and 800 and 52 s for [M0]/[I0] = 400. The longer residence time for the latter case is explained by the placement of the 20 mm conveying element before the kneading elements at the die, extending the backpressure zone of the die and hereby the mean residence time. The final temperature of the extrusion is

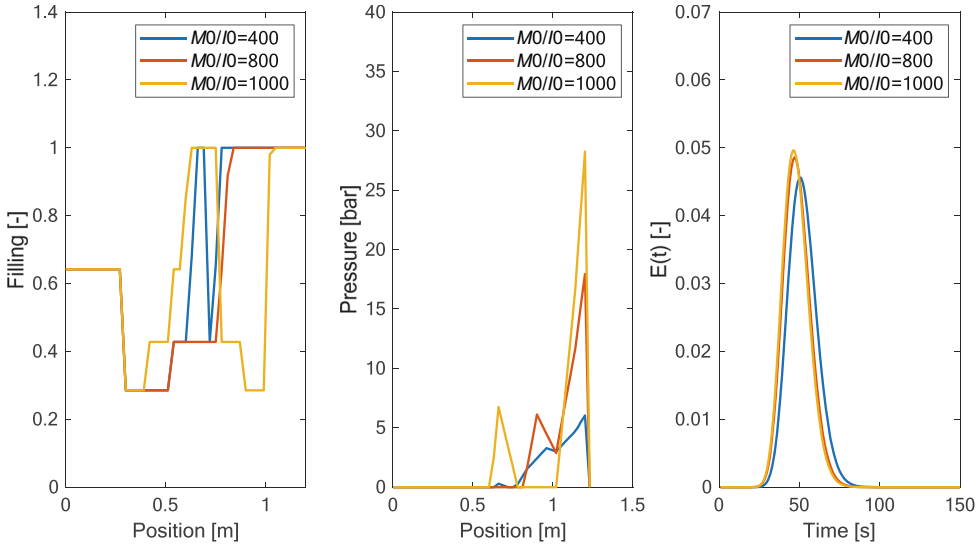

FIGURE 7 Pressure and filling ratio profiles and residence time distribution of the optimal screw configurations.

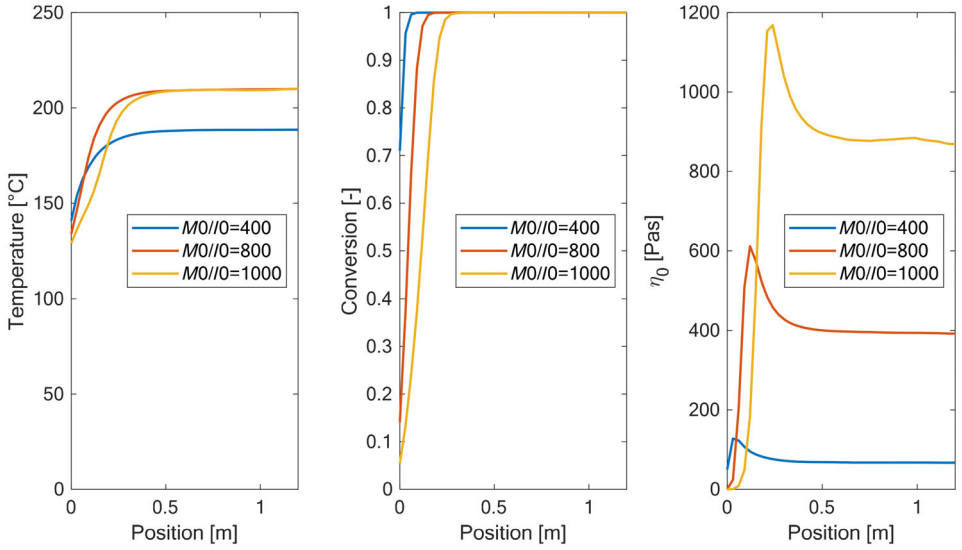

FIGURE 8 Temperature, conversion, and zero shear viscosity profiles of the optimal configurations.

reached after one-third of the extruder length. Caused by the faster reaction for the initiator ratio of 800, the local viscosity is higher causing more viscous dissipation and a faster temperature increase in comparison to the ratio of 1000. Although the reaction rate with a monomer-to-initiator ratio of 400, is faster than in the two previous cases (Equation (26)**)**, the temperature increase is lower due to the lower final molecular weight (Equation (26)) and lower viscosity and viscous dissipation **(**Equation (30)).

In all of the three investigated cases, full conversion is reached at a third of the extruder length due to a sufficiently high temperature and an accelerated reaction speed for higher initiator concentrations (lower initiator to monomer ratios, see Equation (25)). The zero shear viscosity profiles show an initial overshooting of the viscosity for all cases, before reaching the final values. This is due to the reaction progress occurring faster than the temperature increase, as the temperature increase is primarily caused by viscous dissipation.

A comparison of the model with the experimental results from Reference [52] was also carried out. For this, the cases of $[M0]/[I0] = 1000$ with a barrel temperature of 125°C at different throughputs and 100 rpm were simulated for the same screw configuration as in the experimental setup. The mean residence times show a very good accordance. At a throughput of 1.5 kg/h 184 s were simulated (176 s exp.), at 2.4 kg/h 141 s (131 s exp.), and at 3.5 kg/h 118 s (104 s exp.). Our simulation model however predicts significantly higher temperatures (up to 40 K). This is due to the fact that the experimental results were obtained for very low throughputs and rotation speeds. In this case (which our model does not target), the heat transfer coefficient (Equation (15)) is underestimated. Furthermore, the viscous dissipation (Equations (19)–(22)) is overestimated for very low local filling ratios, in this case

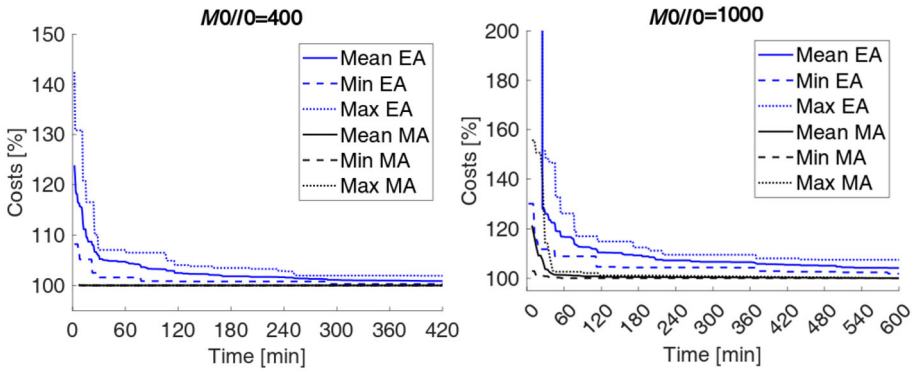

FIGURE 9 Convergence plots of the optimization using the evolutionary algorithm (EA) and the memetic optimization (MA) for the [*M*0]/[*I*0] ratio of 400 (left) and 1000 (right). Shown are the mean, max, and minimum values after each generation of 10 realizations over the total computation time.

Case	Min [%]	Mean [%]	Max [%]	Std. Dev. [%]	Feas. [%]
EA 400	100.8	102.3	103.8	1.040	100.0
EA 800	104.4	107.2	110.8	2.149	78.0
EA 1000	104.4	107.6	109.5	1.813	28.9
MA 400	100.0	100.0	100.0	0.001	100.0
MA 800	100.0	100.1	100.5	0.166	93.7
MA 1000	100.0	100.5	101.1	0.320	56.5

TABLE 8 Results of the memetic optimization (MA) and the optimization only using the evolutionary algorithm (EA) after 180 min of computation time.

only 5%–10%. Our model describes bulk effects, whereas in this experiment other phenomena due to large void spaces dominate. In the throughput range of around 30 kg/h for which the optimizations were performed, these two effects are negligible.

Concluding the validation, the results are coherent with the reference works for the optimization of the process. From an engineering perspective, the process still shows improvement potential as most of the length of the extrusion equipment remains unused and limits the maximum throughput by the constraint on the maximum total mechanical energy input. To apply this method for process optimization at very low throughputs as in the experimental reference work, the thermal process model has to be modified.

4.4 | Performance of the memetic algorithm

In order to quantify the benefit of the MA over a pure EA, it is benchmarked against the optimization using only the evolutionary algorithm. The continuous optimization variables are optimized by the EA in the MA using the mutation and crossover operator, but in contrast to the MA, the continuous variables are not further optimized by the local optimization. The probability of crossover or mutation is parametrized with 20% for each continuous variable in an individual. For three continuous optimization variables, the probability of changes in the continuous variables of the individual is high. For both cases, a population of 25 individuals with an elite percentage of 20% is used. The comparison is performed for the optimization of ε-Caprolactone with different [*M*0]/[*I*0] ratios of 400, 800, and 1000. As the performance metric, the total computation time is used. The optimization was performed on an AMD Ryzen Threadripper 3990X processor. To reduce stochastic effects of the random initialization and in the algorithm, each case was evaluated 10 times. The results are shown in Figure 9. Clearly, the MA outperforms the standard EA.

This finding is further supported by the results shown in Table 8. The performance improvement of the MA compared to the EA increases with higher [*M*0]/[*I*0] ratios. This is partly due to the higher number of feasible solutions in the population, which improves the performance of the MA. Infeasible solutions do not provide the EA with quantitative information on the solution quality. This benefit for highly constrained cases is especially interesting for industrial optimization scenarios, for which multiple operational, quality, and safety requirements have to be met simultaneously. For the case of twin-screw extrusion and especially for reactive extrusion, the continuous variables have a strong effect on the quality of a solution because, for example, a small deviation from the optimal temperature might lead to a violation of the required conversion.

In general, to reduce the optimization time for problems with a large number of degrees of freedom, the search space can be reduced by tightening the operating

window of the continuous variables based on expert knowledge. For complex processes, such as reactive extrusion, with highly coupled variables, a tightening is hardly possible as the optimal operating region is not known a priori and the optimal operating window is very narrow. This is tackled in the proposed MA by exploiting the search space locally with the local optimization and using the gained information in the evolutionary algorithm, but also by exploring the entire space using different initial starting points provided by mutation and crossover.

5 | DISCUSSION

The proposed combination of model and optimizer tackles the challenge of basing the optimization upon an accurate process model, which is computationally more expensive, by the use of an efficient combination of a local solver with an EA to reduce the number of simulation calls. The presented model overcomes the drawbacks stated in Reference [18] of insufficient model accuracy, especially in terms of the description of the mechanical energy dissipation and the correct representation of the flow patterns. In order to obtain a precise prediction of the residence times in the different sections, not only the conveying and pressure characteristics but also the local mixing effects are taken into account as discussed in Section 2.2. In the model, various screw geometries can be taken into account such as mixing elements, shells, or kneading blocks and conveying elements. As the extruder model is fully parametrized by geometrical properties such as diameter, centerline distance, or L/D ratio, the simulation of different equipment configurations is possible. The model can also be adapted to other applications easily as arbitrarily complex reaction kinetics can be integrated and the model can be simulated in forward mode, instead of requiring that all extrusion states converge to the steady state after a number of passes as in Reference [54]. In Section 4, the optimization results for the ε-Caprolactone case with a comparison to the results obtained by Gaspar-Cunha et al.[18] are shown. Both the results for the optimal screw geometry and operating conditions, as well as the predictions of the operating conditions such as the melt temperature at the die show a good accordance to the experimentally validated model by Gaspar-Cunha et al.[18] Due to the availability of information on all variables of the model, arbitrary cost functions can be chosen that represent the real production costs or other goals as, for example, the minimization of the specific energy demand. Also, for example, a combination of energy efficiency and the time to start up the extruder or the time for product changeover could be used. Constraints on the equipment, input variables, or process parameters can be enforced directly in the optimization. Examples for such constraints could be a maximal temperature gradient of the barrel temperature or a maximal melt temperature or shear rate. The higher model complexity increases the computational time and additional constraints reduce the number of feasible solutions. The addition of the local optimization to the evolutionary algorithm increases the speed of convergence by one order of magnitude and significantly increases the fraction of feasible solutions. To increase the computational performance further, it is conceivable to use data-based models that were trained data generated by the model and possibly additional experimental data. This can either be realized as full data-based model or a hybrid model, as presented for the reactive extrusion of nylon 6,6.[55,56]

6 | CONCLUSION

We have presented an improved model of a reactive extrusion process and a flexible and broadly applicable memetic optimization method for its design. Existing models were combined and extended to account for the special requirements of reactive extrusion and a new and more efficient calculation of the pressure profile was proposed. The integration of the BCM enables an accurate quantification of the effects of mixing and kneading elements.

The model and the optimization method were validated for the polymerization of ε-Caprolactone. The memetic optimization strategy is characterized by a fast convergence and an efficient handling of constraints due to the embedding of local optimizations of the continuous degrees of freedom. For the reference case, a speed-up up to one order of magnitude in computation time compared to the optimization using only the evolutionary algorithm was observed. With an increasing complexity of the optimization problem by more constraints and a smaller feasible operating window, the speed-up of the MA is expected to increase even further. As the chemical system and the extrusion system are parametrized independently, this method can be efficiently applied for process scale-up and be adapted to different reaction systems. The use of a dynamic model offers the possibility to further improve the operation during start up and product changeover and to use the model for advanced process control. In future work, the optimization results will be validated experimentally at both pilot and production scale and a

combination of measured process data and the process model described here will be employed for improved process control of the process.

ACKNOWLEDGMENTS

This research was funded by the European Union's Horizon 2020 research and innovation programme under grant agreement No. 820716 SIMPLIFY. (www.spire2030.eu/simplify). Open Access funding enabled and organized by Projekt DEAL.

CONFLICT OF INTEREST STATEMENT

The authors declare no potential conflict of interests.

DATA AVAILABILITY STATEMENT

The presented data of this study is available from the corresponding author upon reasonable request.

ORCID

Maximilian Cegla https://orcid.org/0000-0002-0830-8603
Sebastian Engell https://orcid.org/0000-0002-3125-9846

REFERENCES

1. Xanthos M. In: Xanthos M, ed. *Reactive Extrusion: Principles and Practice*. 1st ed. Hanser Publishers; 1992.
2. Beyer G, Hopmann C. In: Beyer G, Hopmann C, eds. *Reactive Extrusion: Principles and Applications*. Wiley-VCH Verlag GmbH & Co. KGaA; 2017. doi:10.1002/9783527801541
3. Cassagnau P, Bounor-Legaré V, Fenouillot F. Reactive processing of thermoplastic polymers: a review of the fundamental aspects. *Int Polym Process*. 2007;22(3):218-258. doi:10.3139/217.2032
4. Yasuda K, Armstrong RC, Cohen RE. Shear flow properties of concentrated solutions of linear and star branched polystyrenes. *Rheol Acta*. 1981;20(2):163-178. doi:10.1007/BF01513059
5. Mastan E, Zhu S. Method of moments: a versatile tool for deterministic modeling of polymerization kinetics. *Eur Polym J*. 2015;68:139-160. doi:10.1016/j.eurpolymj.2015.04.018
6. de Smit K, Wieme T, Marien YW, van Steenberge PHM, D'Hooge DR, Edeleva M. Multi-scale reactive extrusion modelling approaches to design polymer synthesis, modification and mechanical recycling. *React Chem Eng*. 2022;7(2):245-263. doi:10.1039/d1re00556a
7. Vergnes B, Della Valle G, Delamare L. A global computer software for polymer flows in corotating twin screw extruders. *Polym Eng Sci*. 1998;38(11):1781-1792. doi:10.1002/pen.10348
8. Gimenez J, Boudris M, Cassagnau P, Michel A. Bulk polymerization of ε-Caprolactone in twin screw extruder: a step toward the process control. *Int Polym Process*. 2000;15(1):20-27. doi:10.3139/217.1570
9. Berzin F, Vergnes B. Transesterification of ethylene acetate copolymer in a twin screw extruder: experimental and theoretical approaches. *Int Polym Process*. 1998;13(1):13-22. doi:10.3139/217.980013
10. Poulesquen A, Vergnes B, Cassagnau P, Michel A, Carneiro OS, Covas JA. A study of residence time distribution in co-rotating twin-screw extruders. Part II: experimental validation. *Polym Eng Sci*. 2003;43(12):1849-1862. doi:10.1002/pen.10157
11. Poulesquen A, Vergnes B. A study of residence time distribution in co-rotating twin-screw extruders. Part I: theoretical modeling. *Polym Eng Sci*. 2003;43(12):1841-1848. doi:10.1002/pen.10156
12. Eitzlmayr A, Khinast J, Hörl G, et al. Experimental characterization and modeling of twin-screw extruder elements for pharmaceutical hot melt extrusion. *AIChE J*. 2013;59(11):4440-4450. doi:10.1002/aic.14184
13. Eitzlmayr A, Koscher G, Reynolds G, et al. Mechanistic modeling of modular co-rotating twin-screw extruders. *Int J Pharm*. 2014;474(1–2):157-176. doi:10.1016/j.ijpharm.2014.08.005
14. Kohlgrüber K. *Co-Rotating Twin-Screw Extruder Fundamentals, Technology, and Applications*. Carl Hanser Verlag GmbH & Co. KG; 2008.
15. Choulak S, le Gorrec Y, Couenne F, Jallut C, Cassagnau P, Michel A. A complete dynamic model for twin screw extruders. *IFAC Proc*. 2004;37(1):239-244. doi:10.1016/s1474-6670(17)38738-4
16. Janssen LPBM, Rozendal PF, Hoogstraten HW, Cioffi M. A dynamic model for multiple steady states in reactive extrusion. *Int Polym Process*. 2001;16(3):263-271. doi:10.3139/217.1651
17. Gaspar-Cunha A, Covas JA, Sikora J. Optimization of polymer processing: a review (part I—extrusion). *Materials*. 2022;15(1):1-31. doi:10.3390/ma15010384
18. Gaspar-Cunha A, Covas JA, Vergnes B. Defining the configuration of co-rotating twin-screw extruders with multiobjective evolutionary algorithms. *Polym Eng Sci*. 2005;45(8):1159-1173. doi:10.1002/pen.20391
19. Teixeira C, Covas JA, Stützle T, Gaspar-Cunha A. Multi-objective ant colony optimization for the twin-screw configuration problem. *Eng Optim*. 2012;44(3):351-371. doi:10.1080/0305215X.2011.639370
20. Urselmann M, Engell S. Design of memetic algorithms for the efficient optimization of chemical process synthesis problems with structural restrictions. *Comput Chem Eng*. 2015;72:87-108. doi:10.1016/j.compchemeng.2014.08.006
21. Urselmann M, Barkmann S, Sand G, Engell S. A memetic algorithm for global optimization in chemical process synthesis problems. *IEEE Trans Evol Comput*. 2011;15(5):659-683. doi:10.1109/TEVC.2011.2150753
22. Cegla M, Fage A, Kemmerling S, Engell S. Optimal design and operation of reactive extrusion processes: Application to the production and scale-up of polyurethane rheology modifiers for paints. *Polym Eng Sci*. 2023.
23. Rauwendaal C. *Polymer Extrusion*. Carl Hanser Verlag GmbH & Co. KG; 2014. doi:10.3139/9781569905395.fm
24. Kohlgrüber K, Hepperle J, König T, et al. Optimierter Betrieb und Scale-up von Doppelschnecken-Extrudern. VDI. ed. *Seminar Handout Leverkusen, Ger VDI Wissensforum*. Published online 2012.
25. Brouwer T, Todd DB, Janssen LPBM. Flow characteristics of screws and special mixing enhancers in a co-rotating twin screw extruder. *Int Polym Process*. 2002;17(1):26-32. doi:10.3139/217.1678
26. Bauer H, Matić J, Khinast J. Characteristic parameters and process maps for fully-filled twin-screw extruder elements. *Chem Eng Sci*. 2021;230:116202. doi:10.1016/j.ces.2020.116202

27. Stritzinger U, Roland W, Berger-Weber G, Steinbichler G. Modeling melt conveying and power consumption of co-rotating twin-screw extruder kneading blocks: Part A. Data generation. *Polym Eng Sci*. 2022;62(11):3721-3745. doi:10.1002/pen.26140
28. Stritzinger U, Roland W, Berger-Weber G, Steinbichler G. Modeling melt conveying and power consumption of co-rotating twin-screw extruder kneading blocks: Part B. Prediction models. *Polym Eng Sci*. 2023;63(3):841-862. doi:10.1002/pen.26249
29. Puaux JP, Cassagnau P, Bozga G, Nagy I. Modeling of polyurethane synthesis by reactive extrusion. *Chem Eng Process Process Intensif*. 2006;45(6):481-487. doi:10.1016/j.cep.2005.11.006
30. Elgeti K. A new equation for correlating a pipe flow reactor with a cascade of mixed reactors. *Chem Eng Sci*. 1996;51(23):5077-5080. doi:10.1016/S0009-2509(96)00342-9
31. Levenspiel O. *Chemical Reaction Engineering*. Vol 38. 3rd ed. John Wiley & Sons, Ltd; 1999. doi:10.1021/ie990488g
32. Cegla M, Engell S. Reliable modelling of twin-screw extruders by integrating the backflow cell methodology into a mechanistic model. *Comput Aided Chem Eng*. 2020;48(Proceedings of ESCAPE30):175-180. doi:10.1016/B978-0-12-823377-1.50030-6
33. Roemer MH, Durbin LD. Transient response and moments analysis of backflow cell model for flow systems with longitudinal mixing. *Ind Eng Chem Fundam*. 1967;6(1):120-129. doi:10.1021/i160021a021
34. Eitzlmayr A, Matic J, Khinast J. Analysis of flow and mixing in screw elements of corotating twin-screw extruders via SPH. *AIChE J*. 2017;63(6):2451-2463. doi:10.1002/aic.15607
35. Cegla M, Engell S. Application of model predictive control to the reactive extrusion of ε-Caprolactone in a twin-screw extruder. *IFAC-PapersOnLine*. 2021;54(3):225-230. doi:10.1016/j.ifacol.2021.08.246
36. Ganzeveld KJ, Capel JE, Van Der Wal DJ, Janssen LPBM. The modelling of counter-rotating twin screw extruders as reactors for single-component reactions. *Chem Eng Sci*. 1994;49(10):1639-1649. doi:10.1016/0009-2509(93)E0023-6
37. Kim EK, White JL. Isothermal transient startup of a starved flow modular co-rotating twin screw extruder. *Polym Eng Sci*. 2000;40(3):543-553. doi:10.1002/pen.11185
38. Choulak S, Couenne F, le Gorrec Y, Jallut C, Cassagnau P, Michel A. Generic dynamic model for simulation and control of reactive extrusion. *Ind Eng Chem Res*. 2004;43(23):7373-7382. doi:10.1021/ie0342964
39. Todd DB. SPE ANTEC *Tech Pap*. 1988 34(54).
40. Teixeira C, Covas JA, Berzin F, Vergnes B, Gaspar-Cunha A. Application of evolutionary algorithms to the definition of the optimal twin-screw extruder configuration for starch cationization. *Polym Eng Sci*. 2011;51(2):330-340. doi:10.1002/pen.21801
41. Zhang G, Zhang M, Jia Y. Multi-objective optimization of reactive extrusion by genetic algorithms. *J Appl Polym Sci*. 2015;132(16):1-6. doi:10.1002/app.41862
42. Crepinsek M, Liu SH, Mernik M. Exploration and exploitation in evolutionary algorithms: a survey. *ACM Comput Surv*. 2013;45(3):1-33. doi:10.1145/2480741.2480752
43. Tao G, Michalewicz Z. *Inver-Over Operator for the TSP*. Vol 20. Springer; 1998.
44. Baraglia R, Hidalgo JI, Perego R. A hybrid heuristic for the traveling salesman problem. *IEEE Trans Evol Comput*. 2001;5(6):613-622. doi:10.1109/4235.974843
45. Beyer H-G, Schwefel H-P. Evolution strategies—a comprehensive introduction. *Nat Comput*. 2002;1(1):3-52. doi:10.1023/A:1015059928466
46. Andersson JAE, Gillis J, Horn G, Rawlings JB, Diehl M. CasADi: a software framework for nonlinear optimization and optimal control. *Math Program Comput*. 2019;11(1):1-36. doi:10.1007/s12532-018-0139-4
47. Gimenez J, Boudris M, Cassagnau P, Michel A. Control of bulk ε-caprolactone polymerization in a twin screw extruder. *Polym React Eng*. 2000;8(2):135-157. doi:10.1080/10543414.2000.10744545
48. Gimenez J, Cassagnau P, Fulchiron R, Michel A. Structure and dynamics of melt poly(ε-caprolactone) from inverse rheological calculation. *Macromol Chem Phys*. 2000;201(5):479-490. doi:10.1002/(SICI)1521-3935(20000301)201:5<479::AID-MACP479<3.0.CO;2-F
49. Gimenez J, Cassagnau P, Michel A. Bulk polymerization of ε-caprolactone: rheological predictive laws. *J Rheol*. 2000;44(3):527-547. doi:10.1122/1.551099
50. Berzin F, Tara A, Vergnes B. Optimization and scale-up of starch cationization in a twin screw extruder. *Polym Eng Sci*. 2007;47(6):814-823. doi:10.1002/pen.20759
51. Dubois P, Ropson N, Jérôme R, Teyssié P. Macromolecular engineering of polylactones and polylactides. 19. Kinetics of ring-opening polymerization of ε-caprolactone initiated with functional aluminum alkoxides. *Macromolecules*. 1996;29(6):1965-1975. doi:10.1021/ma951738h
52. Poulesquen A, Vergnes B, Cassagnau P, Gimenez J, Michel A. Polymerization of ε-caprolactone in a twin screw extruder: experimental study and modelling. *Int Polym Process*. 2001;16(1):31-38. doi:10.3139/217.1626
53. Poulesquen A. Contribution to the modelling of reactive extrusion on a twin-screw extruder. Ecole des Mines de Paris 2001.
54. Berzin F. Etude Expérimentale de Modßelisation d'une Opération d'Extrusion Rèactive. Ecole des Mines de Paris 1998.
55. Giudici R, do Nascimento CAO, Beiler IC, Scherbakoff N. Modeling of industrial nylon-6,6 polycondensation process in a twin-screw extruder reactor. I. Phenomenological model and parameter adjusting. *J Appl Polym Sci*. 1998;67(9):1573-1587. doi:10.1002/(sici)1097-4628(19980228)67:93.0.co;2-a
56. Nascimento CAO, Giudici R, Scherbakoff N. Modeling of industrial nylon-6,6 polymerization process in a twin-screw extruder reactor. II. Neural networks and hybrid models. *J Appl Polym Sci*. 1999;72(7):905-912. doi:10.1002/(SICI)1097-4628(19990516)72:73.0.CO;2-7
57. Tayeb J, Vergnes B, Della VG. A basic model for a twin-screw extruder. *J Food Sci*. 1989;54(4):1047-1056. doi:10.1111/j.1365-2621.1989.tb07941.x
58. Kalyon DM, Gotsis AD, Yilmazer U, et al. Development of experimental techniques and simulation methods to analyze mixing in co-rotating twin screw extrusion. *Adv Polym Technol*. 1988;8(4):337-353. doi:10.1002/adv.1988.060080401
59. Vergnes B, Barrès C, Tayeb J. Computation of residence time and energy distributions in the reverse screw element of a

twin-screw extrusion-cooker. *J Food Eng*. 1992;16(3):215-237. doi:10.1016/0260-8774(92)90035-5

60. Booy M. Geometry of fully wiped twin-screw equipment. *Polym Eng Sci*. 1978;18(12):973-984. doi:10.1002/pen.760181212
61. Tadmor Z, Gogos C. *Principles of Polymer Processing*. 1st ed. Wiley; 1979.
62. Booy ML. Isothermal flow of viscous liquids in corotating twin screw devices. *Polym Eng Sci*. 1980;20(18):1220-1228. doi:10.1002/pen.760201808

How to cite this article: Cegla M, Engell S. Optimal design and operation of reactive extrusion processes: Modeling, model validation, and optimization algorithm. *Polym Eng Sci*. 2023; 63(12):4153-4173. doi:10.1002/pen.26515

APPENDIX A

A.1 | COMPARISON OF A THEORETICAL MODELING APPROACH WITH THE PROPOSED MODEL

In the following section, the transformation of the two different modeling approaches is presented. In the rotational-model for twin-screw extrusion proposed by Reference [57–59] the polymer flow is considered as flow through a C-shaped chamber. The velocity profile in this geometry is determined using the two plate model and for this, the Stokes equation is integrated twice. The pressure distribution in radial direction is neglected. The considered channel has a width W of:

$$W = \frac{\cos(\phi) T_s}{n_F}. \tag{A1}$$

The overall flow $\dot{V}$ can be described as[59]:

$$\frac{\dot{V}}{W} = -F_{p_v} \frac{1}{8\eta} \frac{\Delta P}{\Delta \theta} \left(R_e^2 - R_i^2\right) \left[1 - \left(\frac{2R_e R_i}{R_e^2 - R_i^2} \ln\left(\frac{R_e}{R_i}\right)\right)^2\right] + F_{d_v} \frac{1}{2} \Omega R_e \cos(\phi) \left[1 - \left(\frac{R_i^2}{R_e^2 - R_i^2} \ln\left(\frac{R_e}{R_i}\right)^2\right)\right] \tag{A2}$$

with the screw pitch angle ϕ:

$$\phi = \arctan\left(\frac{T_S}{\pi D}\right). \tag{A3}$$

This holds true for $2\pi - 2\psi$ where ψ describes the intermeshing angle. The flows in the intermeshing section are described as pressure flows with a reduced channel width of W^*[59]:

$$\frac{\dot{V}}{W^*} = -F_{p_v} \frac{1}{8\eta^*} \frac{\Delta P^*}{\Delta \theta^*} \left(R_e^2 - R_i^2\right) \cdot \left[1 - \left(\frac{2R_e R_i}{R_e^2 - R_i^2} \ln\left(\frac{R_e}{R_i}\right)\right)^2\right]. \tag{A4}$$

The width of the channel in the intermeshing section W^* is[59]:

$$W^* = W - \alpha R_e \sin(\phi) \tag{A5}$$

and the angle defining the screw flight α[60] results as:

$$\alpha = \frac{\pi}{n_f} - 2\psi. \tag{A6}$$

The intermeshing angle ψ as defined by[60]:

$$\psi = \arccos\left(\frac{C_L}{D}\right) \tag{A7}$$

with the correction factors F_p and F_d. These shape factors represent the reducing effect of the flights between the infinite parallel plates. They can be calculated as[61,62]:

$$F_d = \frac{16W}{\pi^3 H} \sum_{i=1,3,5}^{\infty} \frac{1}{i^3} \tanh\left(\frac{i\pi H}{2W}\right), \tag{A8}$$

$$F_p = 1 - \frac{192H}{\pi^5 W} \sum_{i=1,3,5}^{\infty} \frac{1}{i^5} \tanh\left(\frac{i\pi W}{2H}\right) \tag{A9}$$

with the channel height H[60]:

$$H = R_e - R_i. \tag{A10}$$

Kohlgrüber developed an empirical model describing the flow phenomena with experimentally determined geometric coefficients[14]:

$$\dot{V} = A_1 n D^3 - \frac{A_1}{A_2} \frac{D^4}{\eta} \frac{\Delta p}{\Delta x}. \tag{A11}$$

For conveying elements, Kohlgrüber suggests the approximation[13]:

$$A_{1,\text{approx}} \approx \frac{A_{\text{cr}} T_s}{2D^3}. \tag{A12}$$

It is also possible to determine an expression for A_1 using the model presented by Vergnes[7] by transformation of the equation for completely filled elements. Equating the result of both models:

$$\dot{V}_{\text{conveying,Kohl}} = \dot{V}_{\text{conveying,Vergnes}}, \tag{A13}$$

$$A_1 n D^3 = F_{d_v} \frac{1}{2} \Omega R_e W \cos(\phi) \cdot \left[1 - \left(\frac{R_i^2}{R_e^2 - R_i^2} \ln\left(\frac{R_e}{R_i}\right)^2\right)\right] \tag{A14}$$

with the angular screw rotation speed Ω:

$$\Omega = \pi D n, \tag{A15}$$

$$A_1 n D^3 = F_{d_v} \frac{1}{2} \pi D n \frac{D}{2} W \cos(\phi) \cdot \left[1 - \left(\frac{R_i^2}{R_e^2 - R_i^2} \ln\left(\frac{R_e}{R_i}\right)^2\right)\right], \tag{A16}$$

$$A_1 = F_{d_v}\frac{1}{4D}\pi W\cos(\phi)\left[1-\left(\frac{R_i^2}{R_e^2-R_i^2}\ln\left(\frac{R_e}{R_i}\right)^2\right)\right]. \quad \text{(A17)}$$

The comparison the pressure characteristics yields:

$$\dot{V}_{\text{pres,Kohl}} = \dot{V}_{\text{pres,Vergnes}} + \dot{V}^*_{\text{pres,Vergnes}}, \quad \text{(A18)}$$

$$\frac{A_1}{A_2}\frac{D^4}{\eta}\frac{\Delta p}{\Delta x} = F_{p_v}\left(\frac{W}{8\eta}\frac{\Delta P}{\Delta\theta}+\frac{W^*}{8\eta^*}\frac{\Delta P^*}{\Delta\theta^*}\right)\left(R_e^2-R_i^2\right) \cdot\left[1-\left(\frac{2R_eR_i}{R_e^2-R_i^2}\ln\left(\frac{R_e}{R_i}\right)\right)^2\right] \quad \text{(A19)}$$

with $\Delta\theta\cdot T_s = \Delta x$ and $\eta^* = \eta$:

TABLE A1 Comparison of the two modeling approaches for different extruders and screw elements.

Screw element	24/24[a]	16/16[a]	16/16[b]	25/25[b]	33/33[b]	20/20[c]	42/42[c]
C_L	15	15	21	21	21	26.2	26.2
D	18	18	25	25	25	30.7	30.7
D_i	11.6	11.6	16	16	16	21.3	21.3
n_F	2	2	2	2	2	2	2
T_S	24	16	16	25	33	20	42
A_1	0.356	0.226	0.197	0.308	0.406	0.157	0.398
$A_{1,\text{approx}}$	0.367	0.245	0.179	0.280	0.370	0.156	0.327
$A_{1,\text{vergnes}}$	0.321	0.215	0.143	0.244	0.318	0.159	0.342
A_2	766.5	808.6	832	798	768	1284	1165
$\frac{A_1}{A_2}\cdot 103$	0.464	0.279	0.237	0.386	0.529	0.123	0.342
$\frac{A_{1,\text{Vergnes}}}{A_{2,\text{Vergnes}}}\cdot 103$	0.712	0.299	0.144	0.406	0.730	0.099	0.494
$\frac{A_{1,\text{approx}}}{A_{2,\text{approx}}}\cdot 103$	0.478	0.302	0.215	0.351	0.481	0.187	0.427

[a]Eitzlmayr (2014) Coperion ZSK 18.[13]
[b]Eitzlmayr (2014) Clextral BC21.[13]
[c]Brouwer (2002) Coperion ZSK 30.[25]

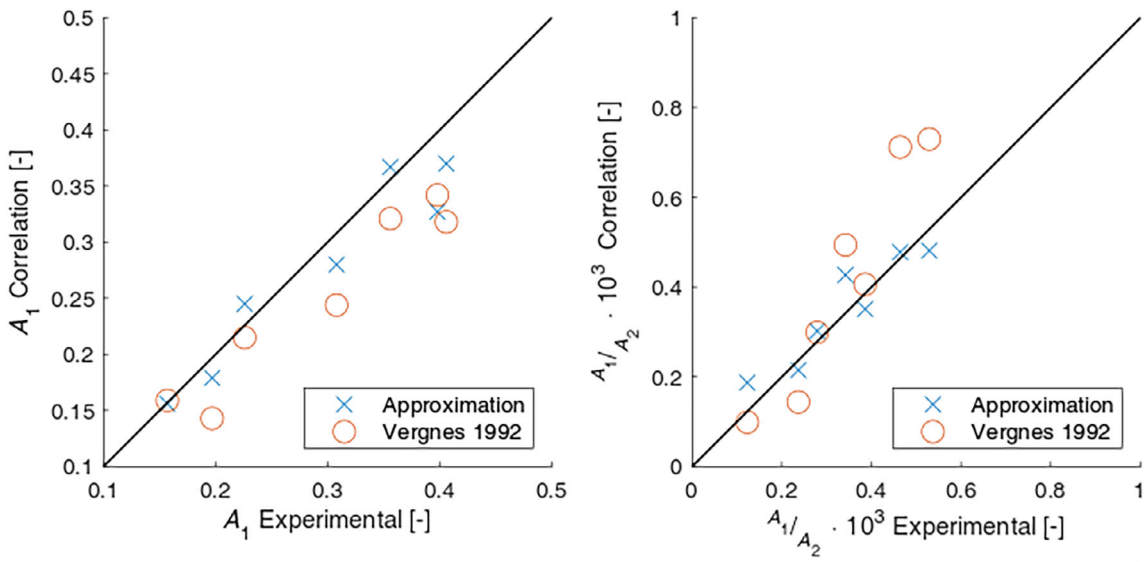

FIGURE A1 Comparison of the experimental conveying flow characteristics (A_1) and the pressure flow characteristics $\left(\frac{A_1}{A_2}\right)$ with the approximations developed by Kohlgrüber and Eitzlmayr and with the theoretical approach developed by Vergnes 1992.

$$\frac{A_1}{A_2} = F_{p_v} \frac{T_s}{8D^4} \left(\frac{W}{2\pi - 2\psi} + \frac{W^*}{2\psi} \right) \left(R_e^2 - R_i^2 \right) \cdot \left[1 - \left(\frac{2R_e R_i}{R_e^2 - R_i^2} \ln\left(\frac{R_e}{R_i} \right) \right)^2 \right]. \quad \text{(A20)}$$

For the approximation of the pressure characteristics Equation (7) is used:

$$A_2 \approx -93.4 \cdot \frac{T_s}{D} + 893. \quad \text{(A21)}$$

The comparison of both results is shown in Table A1 for different element characterizations on different extruders. The results are also shown in Figure A1. For the conveying flows, the agreement of the approximation developed by Kohlgrüber for A_1 with the experimental data is slightly better than the theoretical approach by Vergnes. A possible explanation for this might be that the simplification as two parallel plates without considering the screw curvature. Comparing the prediction performance of $\frac{A_1}{A_2}$, the approximation is significantly better than the theoretical approach. This is caused as five out of the seven points depicted were used to determined the approximation in Equation (A21) and also geometrically similar screw elements in terms of pitch-to-diameter ratio were investigated. In case no a-priori information is available, the theoretical approach using Equation (A20) provides a good first approximation.

A.2 | EXAMPLE FOR THE APPLICATION OF THE INVER-OVER OPERATOR

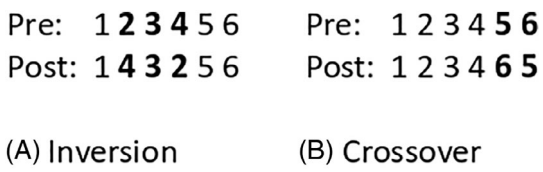

FIGURE A2 Example for the application of the Inver-over operator for inversion (A) and crossover (B). For the inversion (A), the sequence between element 1 and 5 is inverted. For the crossover (B), the sequence of the two adjacent elements 5 and 6 switched.